Wing-Body Interaction: Numerical simulation, Wind-tunnel and In-flight Testing

Lukas Popelka
Institute of Thermomechanics, Academy of Sciences of the Czech Republic, Prague
popelka@it.cas.cz

Lubor Zeleny
Aeroclub Pribyslav, Czech Republic
lubor.zeleny@post.cz

David Simurda
Institute of Thermomechanics, Academy of Sciences of the Czech Republic, Prague
simurda@it.cas.cz

Milan Matejka
Faculty of Mechanical Engineering, Czech Technical University in Prague
milan.matejka@fs.cvut.cz

Presented at the XXIX OSTIV Congress, 6-13 August 2008, Lüsse Germany and at the Soaring Society of America Convention, 30 January 2010, Little Rock AR USA [wwww.youtube.com, search: OSTIV]

Abstract

Wing-body interaction has been investigated by means of numerical simulation (CFD), wind-tunnel and in-flight measurements. Aims of the turbulent separation study, verification of CFD methods and application of flow-control devices have been settled. The sailplane wing-fuselage junction was subjected to in-flight visualization at four airspeeds and video recordings of a tuft array were acquired. Area of boundary layer separation was determined. The speed polar of the test aircraft was measured with an FAI International Gliding Commission approved flight recorder. Simplified geometry, with the empennage removed, was used for CFD modelling and wind-tunnel visualization. Analysis of both numerical and experimental data confirms lift-distribution distortion induced by the presence of the fuselage. Passive flow-control devices were used in the junction and in-flight visualization proved turbulent separation suppression and positive influence on the sailplane performance was measured at thermalling speeds with degradation at higher speeds. Consequently, new layout of passive devices was developed but has yet to be fully verified.

Nomenclature

cp	pressure coefficient	-
c	chord length	m
H	normalised helicity	-
L/D	glide ratio (lift/drag)	-
Re	Reynolds number	-
S	rate of strain tensor	1/s
Tu	intensity of turbulence	-
v	longitudinal velocity	m/s
w	velocity vector	m/s
Axis		
x	Longitudinal	
z	Spanwise	
Greek symbols		
α	angle of attack	deg
ω	vorticity vector	1/s
Ω	vorticity tensor	1/s
Subscripts		
i, j	Components	

Introduction

In order to investigate and understand the extent of the wing-body interaction effects taking place during the operation of a particular self-launching sailplane, several measurements and CFD calculations were performed. According to the obtained data, a passive flow-control device was placed on the wing close to fuselage to suppress separation of a boundary layer and to improve sailplane performance under certain flight conditions. Improvement of the performance has been assessed through measurements of the speed polar. Investigations were performed at airspeeds ranging from 80 km/h to 160 km/h to cover range of velocities common for this class of sailplane. Special attention was paid to airspeed 85 km/h which corresponds to thermal flight.

Wing-body interaction effects

Much attention has been devoted to flow phenomena occurring in region of a wing-fuselage junction. According to Schlichting and Tuckenbrodt[1] and Boermans and Terleth[2], the main aerodynamic effects of wing-fuselage interference consist of:

i) Displacement effects taking place due to spanwise curvature of the intersection lines between the wing and fuselage. As a result streamwise velocity distribution on the wing changes towards the fuselage.

ii) Effects of asymmetry, i.e. the difference between the wing-fuselage intersection lines of the upper and lower surface. Intersection lines differ when the wing is shifted to a high wing or low-wing position, when the wing is cambered or set at incidence angle relative to fuselage. If the fuselage is of a cylinder-like shape, this leads to change of velocities on both sides of the wing according to particular geometrical setup.

iii) Lift effects originate from interaction of circulatory flows around the wing and the fuselage. Upwash in front of the wing and downwash behind the wing are influenced by additional fuselage crossflow velocity (alpha flow) at the junction. If both a cylindrical fuselage and the wing in mid-wing position are at positive angle of attack, then due to alpha flow, the angle of attack at the wing root is higher.

iv) Effects of viscosity results in flow separation and generation of vortices. Due to strong adverse pressure gradient in front of the wing root leading edge, the boundary layer on the fuselage separates from the surface along a separation line thus forming a horseshoe vortex. Both the upper and lower branches of this vortex spread streamwise along the wing root. Due to induced angle of attack and usually divergent shape of the junction, the location of the boundary layer transition on the wing shifts upstream closer to the junction forming a turbulent wedge. This leads to flow separation at higher angles of attack.

Geometry subject to the investigation

The study was initiated by in-flight measurements on a particular self-launching TST-10a sailplane, call-sign OK-A631 /LZ/ (Fig. 1). It is a single-seat composite-structure sailplane with fixed undercarriage and a retractable propulsion unit. The main dimensions of the TST-10a wing are presented in Fig. 2.

The fuselage shape followed published coordinates[2] (Model No. 1) and, together with a Wortmann FX66 series wing airfoil[3], created a suitable test case for this interaction investigation.

The geometry of the computational model was simplified in comparison to the real aircraft (Fig. 3) - the empennage was omitted and only the inner part of the wing was considered, having a simplified rectangular planform. Also, the small fillet in the junction of the wing and the fuselage was neglected to make easier the preparation of the mesh.

The 1:5 scale wind-tunnel model (Fig. 4) was based on the previously mentioned geometry for CFD. The span was reduced to fit the height of the test section. The fillets of the real geometry were retained.

Numerical modelling

Commercial code Fluent 6.3 was used for numerical simulation of flow past a simplified model of TST-10a in order to investigate 3D effects and distortions of pressure and velocity distributions taking place in the junction of the body and the fuselage. Several methods were used to identify vortex structures originating due to interference effects in this part of the aircraft.

Computational model

Geometry of the model was created based on fuselage and airfoil coordinates. The whole computational domain with applied types of boundary conditions can be seen in Fig. 5.

In order to ensure accurate results and to keep computational costs as low as possible, a hexahedral grid was used for meshing of the computational domain (Fig. 6). The mesh was refined at walls. Due to problems with geometry, however, the laminar sub-layer was not resolved everywhere in the domain. The maximum value of y^+ was 17.

Flow properties at the inlet were characterized by an inlet velocity v of 23.6 m/s (85 km/h), hence Re_c equalled $1.5 \cdot 10^6$ and the inlet turbulence intensity Tu was 0.2%. Straight flight was modelled, hence, the angle of attack of the wing α was 4 deg. Outlet to atmospheric pressure at turbulence intensity Tu of 0.2% was considered at the exit from the domain. The second order accuracy scheme was used for discretization of governing equations. Turbulent flow was modelled using realizable k-ε model of turbulence[4], which performs well in flows involving rotation, boundary layers under strong adverse pressure gradients, separation and recirculation. Spalart-Allmaras and sst k-ω turbulence models[5, 6] were assessed as well. The effect on the analysed results, however, was insignificant. Near-wall flow was modelled using a combination of a two-layer model and wall functions.

Methods of vortex identification

Since some of the effects taking place at the fuselage-wing junction results in generation of vortex structures, these structures needed to be identified in the flowfield. There exist numerous methods of vortex identification. Those methods used in this research are described below.

Mapping of streamlines onto a plane normal to the vortex core

A structure is called a vortex when instantaneous streamlines mapped onto a plane, normal to the vortex core, exhibit roughly a spiral or circular pattern when viewed from a reference frame moving with the centre of the vortex core[7].

Q-criterion

A vortex exists in locations where rotation dominates over strain. The second invariant of velocity gradient Q is positive in such locations:

$$Q = \frac{1}{2}\left(\Omega_{ij}\Omega_{ij} - S_{ij}S_{ij}\right) \tag{1}$$

$$Q \geq Q_{th} \tag{2}$$

Normalized helicity

The angle between the velocity vector and the vector of vorticity is zero in the vortex core. Normalized helicity is defined as a cosine of this angle:

$$H_n = \frac{w_i \cdot \omega_i}{|w_i| \cdot |\omega_i|} \quad (3)$$

Hence the vortex core is defined as

$$|H_n| = 1. \quad (4)$$

Results of numerical modelling

The distribution of static pressure on the wing and the fuselage (Fig. 7) shows an increase of static pressure on the wing upper surface as the fuselage is approached. This is a consequence of the displacement effect mentioned previously in paragraph ii) on page 30. Distributions of the pressure coefficient c_p along wing sections at various distances from the fuselage were evaluated and are shown in Fig. 8. Distribution curves of sections at locations closer to the fuselage are incomplete as a result of the junction geometry. This also is the reason for the displacement effect. A decrease of values of c_p closer to the junction is evident.

Notice in Fig. 8 the shift of the stagnation point location in the chordwise direction in case of the section located at z = 0.248 m. This stagnation point shift quantitatively describes effects of "alpha flow", whose consequence is an increase of the angle of attack of the wing in close proximity to the fuselage. The difference between the angle of attack of flow undisturbed by the fuselage and the flow in close proximity to the fuselage (z = 0.248 m) is 30 deg. The whole situation is well visualized by distribution of static pressure in Fig. 9.

Generation of the horseshoe vortex can be seen in Fig. 10. Streamlines in the picture are mapped onto a plane perpendicular to the wing surface in the region of the stagnation point. It can be clearly seen how the boundary layer on the fuselage surface separates and forms the vortex as described in paragraph ii) on page 30. Also, another much smaller contrarotating vortex is observed closer to the leading edge. Contours of the total (over)pressure indicate that the boundary layer thickness prior to the vortex generation was approximately 30 mm. Such a value of the boundary layer thickness is rather high, since the whole flow was considered to be turbulent.

Further development of the horseshoe vortex is illustrated in Fig. 11 which shows contours of Q in planes perpendicular to longitudinal axis of the model. Planes are located in longitudinal positions 0.01, 0.49, 0.71, 1.14, 1.57, 2.22, 3.08, 3.94 of x/c with respect to the leading edge. It can be seen both branches, upper and lower, more or less follow the upper and lower surfaces of the wing and stretch further downstream. Detail of the two vortex branches can be seen in Fig. 12.

Another viscous effect - flow separation - was not predicted by the simulation, although the steep pressure gradient on the upper surface behind x/c = 0.4 (Fig. 8) would suggest so. As it will be mentioned later, wind-tunnel and in-flight tests proved the flow separated on the upper surface of the wing close to the fuselage. The reason why the numerical simulation failed to predict flow separation is probably due to inadequately refined mesh on the surface of the wing. Cells with the highest value of y^+, 17, were located just on the upper surface of the wing.

In-flight measurements

Methods

Standard pressure instruments and GPS-based technologies were used for data acquisition. The altimeter and airspeed indicator were connected to factory-designed static ports located 1780 mm aft of the fuselage nose and 250 mm above its lower surface contour. A thermocouple was placed outside the canopy frame to measure the flow temperature. GNSS Flight Recorder LX20 was used to acquire GPS signals. The recorded flight track was post-processed and the evaluated flight speed and sink rate were reduced to the International Standard Atmosphere. Calibration of the sailplane pitot-static system was obtained.

Oil flow visualisation at two positions along wingspan was obtained. Oil was applied on the surface prior to take-off and a flight of 10 minutes duration was carried out. The airspeed V of 100 km/h IAS was held constant during the whole flight, even during the climb and approach to landing.

An array of tufts was applied to the wing root area as seen in Fig. 13. The tufts were uniformly distributed in three lines. Each of the two outer lines contained 7 tufts and the inner line contained 6 tufts.

Video recording by a camera located on the tail-boom was acquired. To cover the common competition range, airspeeds V of 85, 100, 130 and 160 km/h IAS were selected. The extent of separation was studied in these conditions in straight flight to prevent sideslip which was not modelled in the CFD simulations and in the wind-tunnel sessions.

Measurement of the TST-10a sailplane speed polar was based on GPS methodology[8] which was further refined. Every measurement programme was started at an altitude of 2000 m AGL or higher. Four individual straight flight sequences were used for each airspeed. Flight tracks of 300 m altitude-loss in each sequence were recorded.

Results

The region of the separation bubble was determined using oil flow visualization on the lower wing surface. This region can be seen in Fig. 14 as the dark area where the oil remained accumulated due to significantly lower surface friction.

Based on previous findings, gained with a Standard Cirrus sailplane[8] which led to 10.7% glide ratio L/D improvement of OK-7077 /CX/ at V of 115 km/h IAS, zig-zag type turbulators were applied along the wingspan.

Tuft visualization in the region of the wing-fuselage revealed a region of separated flow at V of 85 km/h IAS. A counter-rotating vortex generator of height h of 3mm (denoted as VG1) was applied in chordwise location

x/c of 0.48. Subsequent flight tests proved suppression of the separation (Fig. 15).

Effect on the performance was established by measuring both the uncontrolled and controlled speed polar of the test sailplane as presented in Fig. 16. Measured glide ratio curves are plotted along with theoretical curve[6].

It can be seen in Fig. 16, installation of the wing-root vortex generator VG1 resulted in a L/D improvement in the low-speed range. Compared to the theoretical curve, it can be seen that a notable shift towards improved TST-10 performance has been achieved. The remaining difference was due to the drag of fixed main undercarriage.

On the other hand, a substantial decrease of L/D was measured for typical interthermal glide airspeed. This unacceptable deterioration of high-speed sailplane performance has lead to the new layout of vortex generator VG2 and cited unfavourable feature was supressed. Low-speed performance remains to be tested thoroughly.

This result illustrates the change of the boundary layer properties, related to airspeed, have to be taken in account and the dimension of vortex generators has to be carefully optimised.

Wind-tunnel measurements

The closed-circuit, closed test section, research wind-tunnel of the Institute of Thermomechanics Academy of Sciences CR was used for tuft visualization on a 1:5 scale model.

A test section of dimensions $865 \times 485 \times 900$mm was designed for airfoil and wing-body investigations[9]. Circular end plates provide an attachment for both types of models. The turntables are 500 mm in diameter and are flush with the wind-tunnel walls. They are electrically driven to enable angle of attack changes for the model. The airfoil was mounted so the center of rotation of the circular plates was at 40% of the model chord. The same fraction is preserved for the body model with respect to wing chord. The air gaps at the tunnel walls were sealed by labyrinth packing.

Visualizations, carried out for five angles of attack, confirmed the formation of a separation zone in the studied area and also revealed the flow structure in the stalled regime as shown in Fig. 17. The model was prepared, also, for static pressure distribution measurements. Note the line of orifices upstream the tuft array in Fig. 17.

Conclusions

Numerical calculations helped to investigate the flow structures in the wing-fuselage junction to some extent. The calculated flow-field in the junction region embodied displacement and lift effects and viscous effects represented by a horseshoe vortex. Separation visualised during wind-tunnel and in-flight testing, however, was not observed, although, geometry simplifications of the computational model (no fillets, no fairing) were "separation friendly". To correct this shortcoming, the computational mesh needs to be refined in the near-wall region which will lead to further extension of pre-processing and calculation time. Nevertheless, even the initial approach presented here is still too demanding to be easily employed in an optimization task sought for sailplane design.

Methodology of flow visualisation feasible for in-flight investigation on airfoils and bodies was employed. Sailplane speed-polar measurement with the GNSS Flight Recorder was further improved.

The insight into the separated flow structure has been improved by the wind-tunnel tuft visualization.

Two types of passive flow-control devices were used. For boundary layer transition control, the optimum location of standard (in-line) zig-zag turbulator was established. The case of turbulent separation control has shown potential performance improvement with (stand-alone) vortex-inducing devices. Installation of the wing-root vortex generator VG1 resulted in a sailplane L/D improvement in the low-speed range but a substantial decrease of L/D was measured for typical interthermal glide airspeed.

This result demonstrated the need for an effective passive flow-control device, with minimized off-design detrimental effects. In the given wing-fuselage geometry, application of an acoustic-driven synthetic jet may be feasible. Such an active device could be optimized to supress separation at V of 85 km/h IAS. For higher airspeeds, the jet intensity should be lowered with dynamic pressure as a trigger and, hence, adaptive control may be reached.

All successful modifications to the TST-10 sailplane, such as new winglets, turbulators and vortex generators, have found application in series production.

Acknowledgments

The work has been supported by Ministry of Education, Youth and Sports of the Czech Republic within project No. 1M06031. Support by the Czech Science Foundation under grants No. IAA2076403 and No. GA 101/08/1112 is gratefully acknowledged.

References

[1]Schlichting, H. and Truckenbrodt, E., *Aerodynamics of the Airplane*, 1st ed., McGraw-Hill, New York, 1979.

[2]Boermans, L.M.M. and Terleth, D.C., "Wind-tunnel Tests of Eight Sailplane Wing-Fuselage Combinations", *Technical Soaring*, Vol. 8, No. 3, 1984, pp. 70-85.

[3]Althaus, D., and Wortmann, F.X., *Stuttgarter Profilkatalog I*, 1st ed., Vieweg & Sohn Verlagsgesellschaft, Braunschweig, 1981.

[4]Shih, T.-H., Liou, W. W., Shabbir, A., Yang, Z. and Zhu, J., "A New k-epsilon Eddy-Viscosity Model for High Reynolds Number Turbulent Flows - Model Development and Validation", *Computers Fluids*, 24(3):227-238, 1995

[5]Spalart P. and Allmaras, S., "A one-equation turbulence model for aerodynamic flows", Technical Report AIAA-92-0439, American Institute of Aeronautics and Astronautics, 1992

[6]Menter, F. R., "Two-Equation Eddy-Viscosity Turbulence Models for Engineering Applications", *AIAA Journal*, 32(8):1598-1605, August 1994

[7]Robinson, S. K., "Coherent Motions in the Turbulent Boundary Layer", *Annual Review of Fluid Mechanics*, Vol. 23., 1991, pp. 601-639.

[8]Popelka, L., "Aerodynamic Optimization of Sailplane Airfoils", Ph.D. Dissertation, Department of Fluid Dynamics, Czech Technical University in Prague, 2006.
[9]Popelka, L., "Wind Tunnel Test Section for Aifoils and Bodies, Research Programme Feasibility Studies", *Proceedings of the Conference Topical Problems of Fluid Mechanics 2008*, Institute of Thermomechanics AS CR , Prague, 2008, pp. 85-88.

Figure 1 Test aircraft TST-10a (OK-A631 /LZ/).

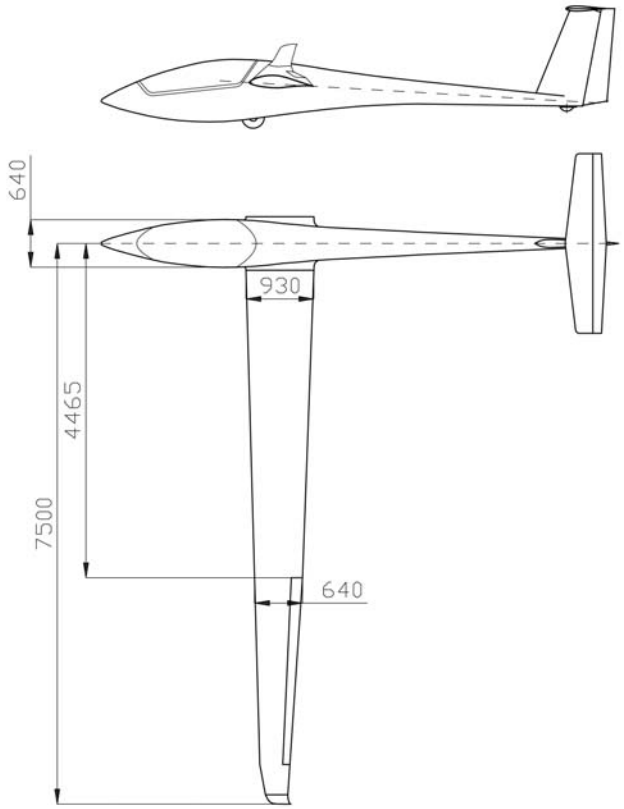

Figure 2 Test aircraft TST-10a (OK-A631 /LZ/) - main dimensions.

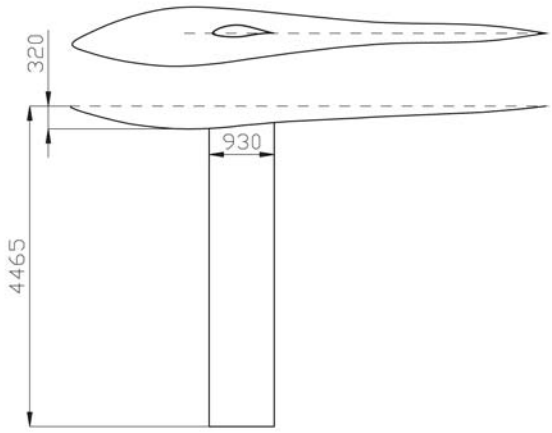

Figure 3 Sketch and dimensions of the geometrical model used for CFD calculations.

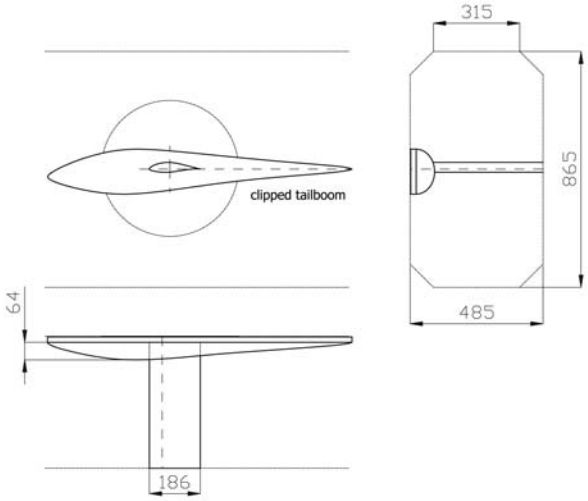

Figure 4 Sketch and dimensions of the model used for wind-tunnel testing.

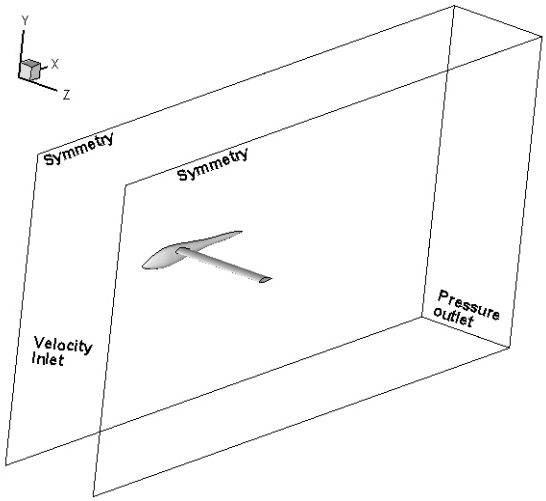

Figure 5 Scheme of the computational domain with boundary condition types.

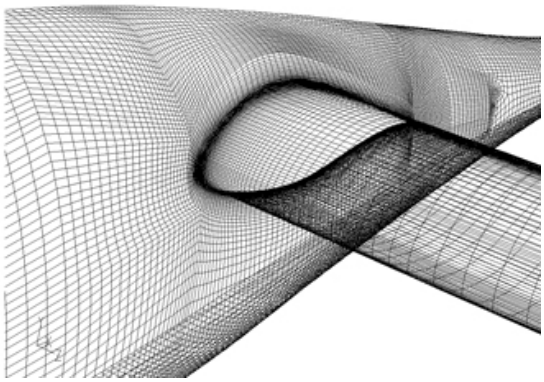

Figure 6 Mesh of the computational domain

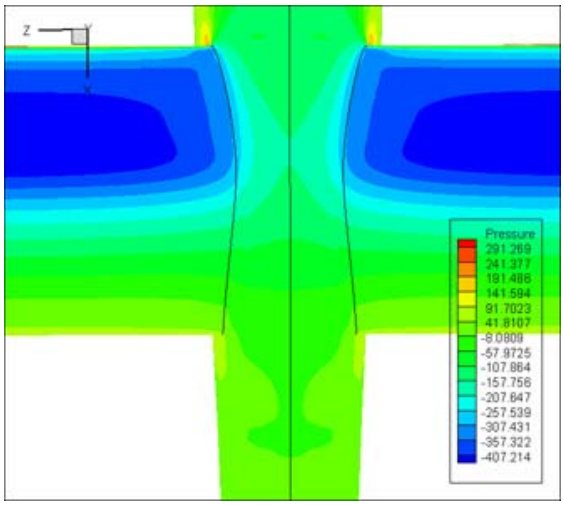

Figure 7 Static (over)pressure distribution on the fuselage and the wing.

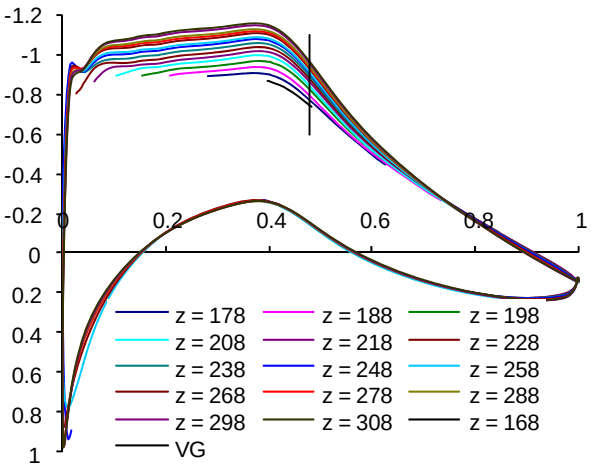

Figure 8 Distributions of cp along wing sections located at different distances from the fuselage (z coordinate). Location of vortex generator (VG) used in in-flight tests.

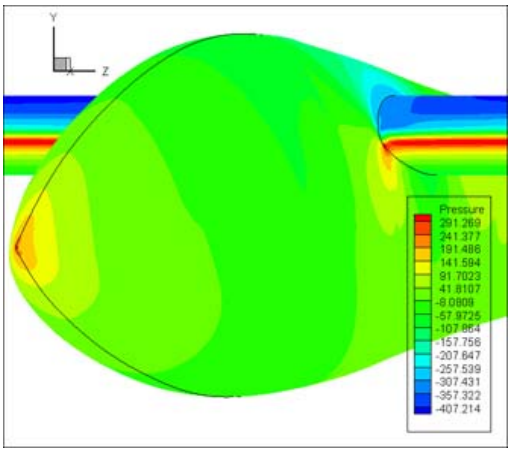

Figure 9 Static (over)pressure distribution on the fuselage and the wing.

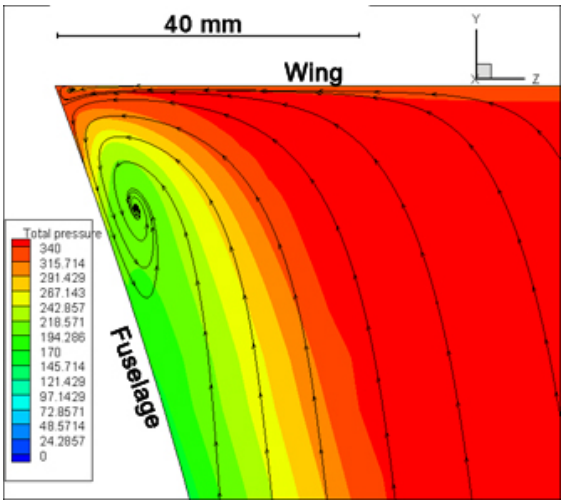

Figure 10 Streamlines mapped onto a plane perpendicular to the wing surface with contours of total (over)pressure.

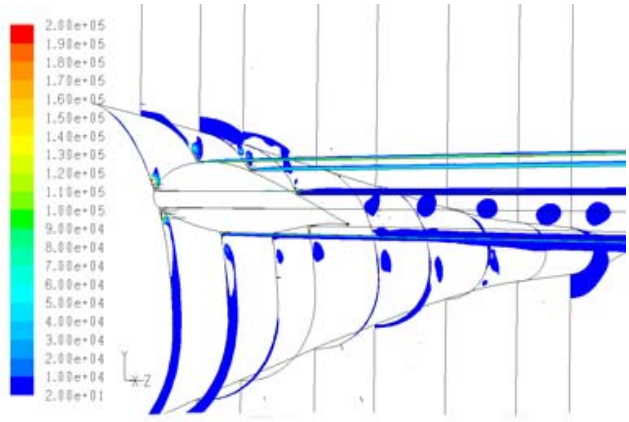

Figure 11 Contours of Q in planes perpendicular to longitudinal axis of the model showing development of the horseshoe vortex.

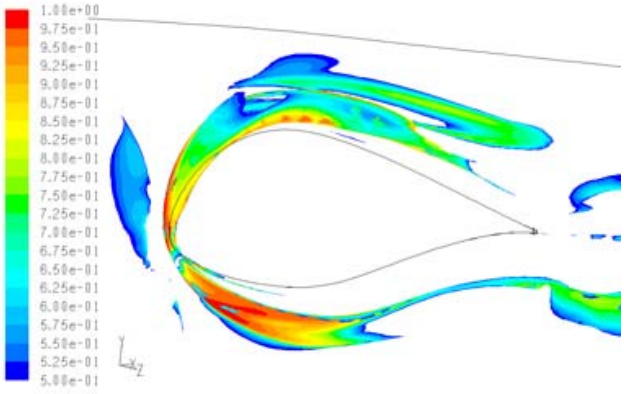

Figure 12 Iso-surface of Q = 10 covered with contours of absolute helicity ranging from 0.5 to 1.

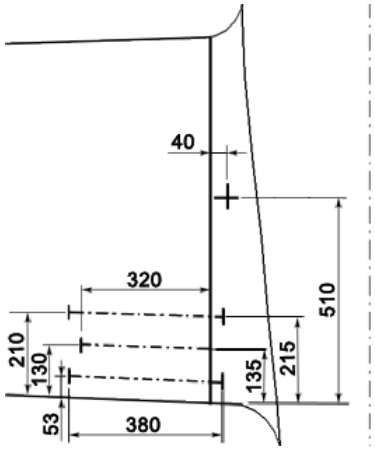

Figure 13 Scheme of distribution of tufts in the wing root area and position of vortex generator.

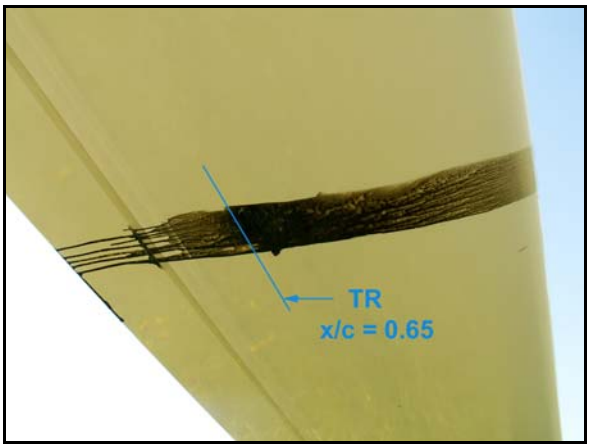

Figure 14 Oil-flow visualization on lower surface of outer wing segment in the aileron region. V = 100 km/h IAS. Right to left: laminar boundary layer, separation bubble, turbulent reattachment (TR).

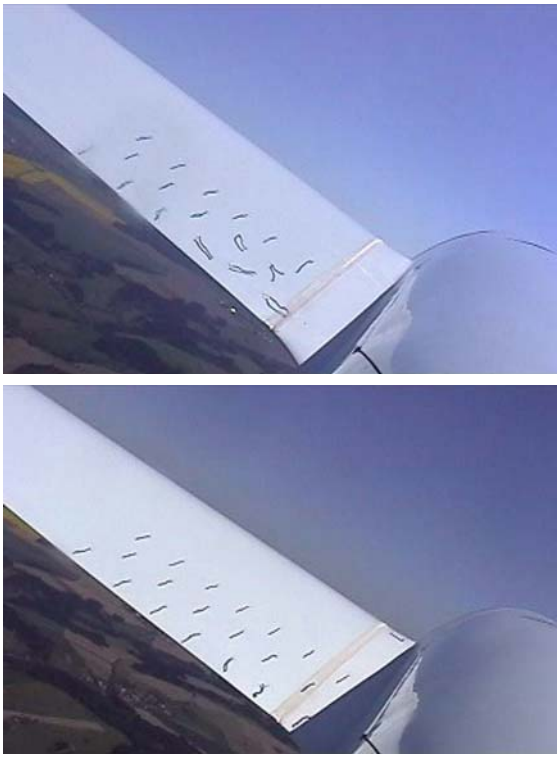

Figure 15 Tuft visualization on the left wing root (V = 85 km/h) IAS. Top – uncontrolled case, Bottom – VG1 applied.

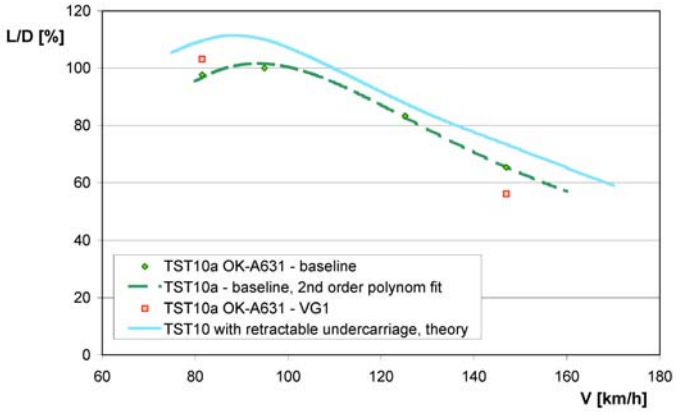

Figure 16 Measured L/D performance of TST10a sailplane.

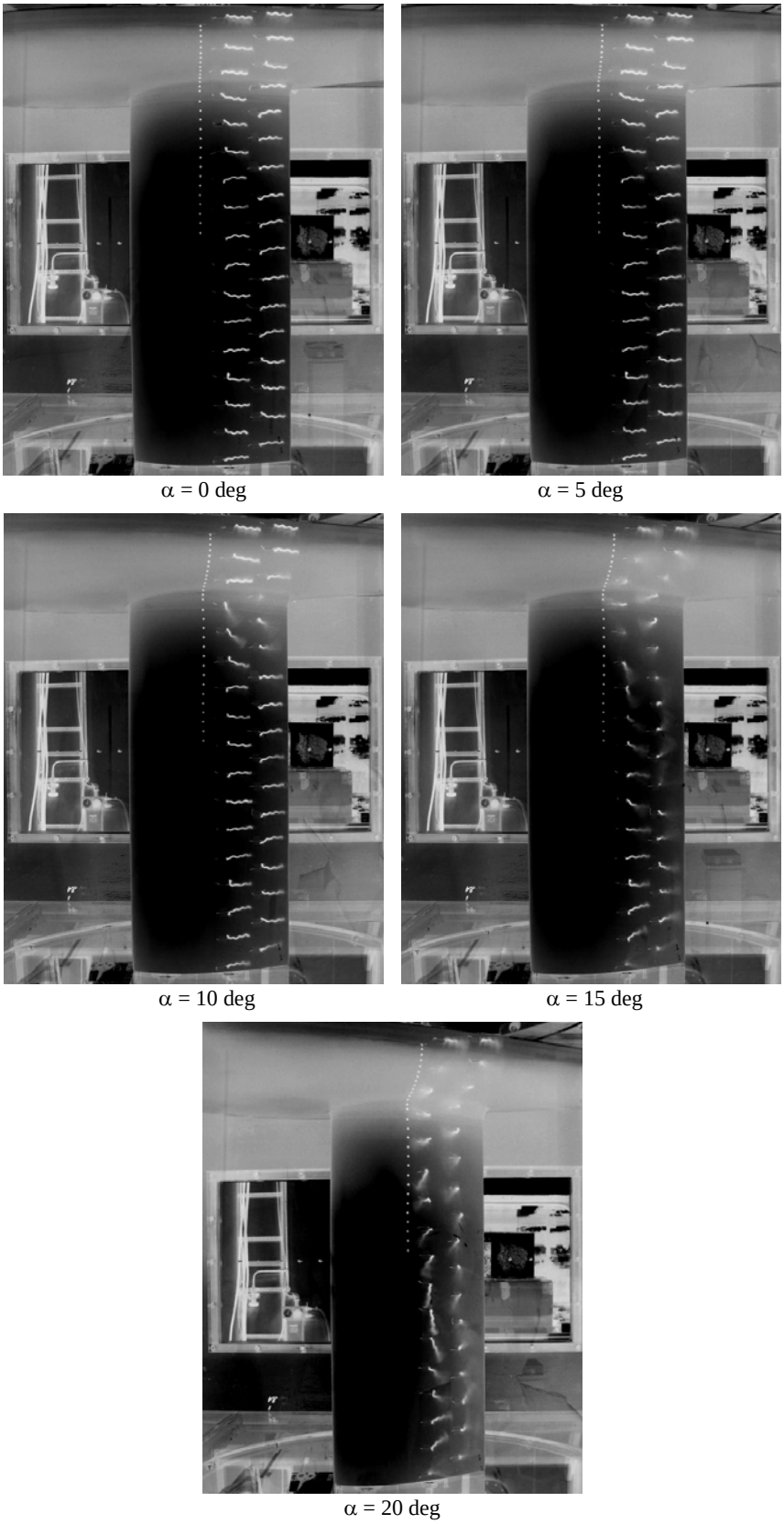

Figure 17 Tuft visualization in CAT 865 x 485 x 900 mm wind-tunnel test section on 1:5 scale model, $Re_c = 2 \cdot 10^5$. Long-exposure inverted photographs of the upper surface.